

# Effect of Ammonium Formate Addition on Corrosion Behavior of Trivalent Chromium Coatings Electrodeposited in Deep Eutectic Solvents

Hung-Hua Sheu<sup>1,2,\*</sup>, Tzu-Te Lin<sup>3</sup>, Ming-Der Ger<sup>1,2,\*</sup>

<sup>1</sup> Department of Chemical and Materials Engineering, Chung Cheng Institute of Technology, National Defense University, Taoyuan City, Taiwan

<sup>2</sup> System Engineering and Technology Program, National Yang Ming Chiao Tung University, Hsin-Chu, Taiwan

<sup>3</sup> Graduate School of National Defense Science, Chung Cheng Institute of Technology, National Defense University, Taoyuan City, Taiwan

\*E-mail: [shhccit@gmail.com](mailto:shhccit@gmail.com), [mingderger@gmail.com](mailto:mingderger@gmail.com)

Received: 9 January 2022 / Accepted: 25 February 2022 / Published: 6 June 2022

The Cr thin films were electrodeposited from trivalent chromium deep eutectic solvents. The conditions of deep eutectic solvents divided into without water (specimen C1), added 15 wt% water (specimen C2), added 15 wt% water with ammonium formate (specimen C3). The HR-TEM shows the structure of "C1" is amorphous structure, and both "C2" and "C3" belong to nano-crystalline structure. The best corrosion resistance of Cr thin film is "C3" which  $i_{\text{corr}}$  value is approximately at  $3.69 \times 10^{-7} \text{ A/cm}^2$ , the worst corrosion resistance of Cr thin film is "C1" which  $i_{\text{corr}}$  value is approximately at  $3.05 \times 10^{-5} \text{ A/cm}^2$ , it can be attributed to "C3" has a dense structure and "C1" has a loose structure. The EIS analysis also presents "C3" has the best corrosion resistance. The reason for the large difference in corrosion resistance can be attributed to the loose structure of the "C1" thin film and the gaps of film is perpendicular to substrate, the dense structure of the "C3" thin film can effectively protect the substrate. Moreover, the addition of ammonium formate into trivalent chromium deep eutectic solvents will promote the reduction reaction of Cr ions and form a dense film.

**Keywords:** deep eutectic solvents, EIS analysis, ammonium formate

## 1. INTRODUCTION

Compared with the traditional electroplating process, in the last two decades, a new kind of ionic liquids has been suggested which is referred to as deep eutectic solvents (DESs), and to be applied on surface treatment field [1]. Deep eutectic solvents is a eutectic mixture composed of the hydrogen bond donor and recipient at a certain stoichiometric ratio by hydrogen bond [2]. Different from the general

aqueous solution plating solution, deep eutectic solvents has some advantages such as higher thermal fixation, good stability to water and atmosphere, non-toxic, biodegradable and biocompatible, so they are considered a green solvent [3,4]. In surface treatment coatings, electrodeposited chromium coatings are widely used in industry due to its excellent corrosion resistance and mechanical properties. But traditional hexavalent chromium baths has highly toxic will cause serious environmental pollution, therefore, recently the much less toxic trivalent chromium solutions are developed to substitute hexavalent chromium baths [5-8]. The previous studies of trivalent chromium electrodeposited from deep eutectic solvents focus on the electrochemical reaction mechanism of deep eutectic solvents bath and seldom to analyze and discuss the structure evolution of the trivalent chromium coatings via electroplating process, especially the effect water adding into the deep eutectic solvents [9-13]. Although the addition of water helps the electrical conductivity of the deep eutectic solvent and promotes the reduction of trivalent chromium ions to metallic chromium, but the reduction of chromium ions to metallic chromium is still not good [14]. In the past studies of trivalent chromium electrodeposition in aqueous systems, it was pointed out that the use of formic acid as a complexing agent can effectively promote the reduction of trivalent chromium ions to metallic chromium [6, 15, 16]. Therefore, adding ammonium formate into the deep eutectic solvent should also obtain the effect of promoting the reduction reaction of chromium ions.

In the early 1990s, Emil Warburg introduced the concept of diffusional impedance into the basic theory to describe the relationship between potential and current when the electrochemical system is in mass transfer control, and then Randles used the equivalent circuit to simulate the charge in the electrochemical system [17]. The impedance values of charge transfer and electric double layer establish a basis for electrochemical impedance spectroscopy in electrochemical analysis technology, so that this technology can be widely used in various electrochemical analysis and corrosion mechanism research. Different from the general polarization corrosion analysis, electrochemical impedance spectroscopy (EIS) analysis technology has been maturely applied to measure the corrosion resistance value of the coating during the corrosion process.

In this study, the choline chloride deep eutectic solvents of trivalent chromium are used to electrodeposit chromium coatings with adding ammonium formate and without ammonium formate in the deep eutectic solvents. The obtained chromium coatings are analyzed using XRD, SEM, TEM and XPS to study the microstructure evolution of chromium coatings effect by the added water in the deep eutectic solvents. Moreover, the corrosion behavior of trivalent chromium electrodeposited conditions are also studied using polarization corrosion analysis and EIS analysis.

## 2. EXPERIMENTAL

The copper sheet are used as a substrate with a dimension of  $25 \times 25 \times 2$  mm, to electrodeposit trivalent chromium coating in the deep eutectic solvents. The chemical composition of deep eutectic solvents is choline chloride and ethylene glycol which mole ratio is 1:2, the addition quantity of main salt ( $\text{CrCl}_3 \cdot 6\text{H}_2\text{O}$ ) is 0.4 mole. The conditions of deep eutectic solvents divided into without water, added 15 wt% water, added 15 wt% water with ammonium formate, the sample code of electrodeposited

coating is called “C1”, “C2” and “C3”, respectively. The parameters of electroplating process is as following: temperature keep at 25°C with a stirring speed at 400 rpm, current density is at 15 A/dm<sup>2</sup> and electroplating for 15 min (the electrodeposited parameters was also shown in Table 1).

**Table 1.** Plating bath composition and operating conditions

Composition and operating conditions			
Sample code	C1	C2	C3
CrCl <sub>3</sub> ·6H <sub>2</sub> O	0.4 mol	0.4 mol	0.4 mol
Choline chloride	1.0 mol	1.0 mol	1.0 mol
Ethylene glycol	2.0 mol	2.0 mol	2.0 mol
Added content of H <sub>2</sub> O	none	15 wt. %	15 wt. %
Added content of ammonium formate	none	none	0.5 mol
Temperature	25°C	25°C	25°C
Stirring speed	400 rpm	400 rpm	400 rpm
Current density	15 A/dm <sup>2</sup>	15 A/dm <sup>2</sup>	15 A/dm <sup>2</sup>
Electroplating time	15 min	15 min	15 min

The phase identification of trivalent chromium coatings were examined by a X-ray diffractometer (XRD, BRUKER D2 PHASE) using Cu K $\alpha$  radiation ( $\lambda=0.15405$  nm) with a scanning range from 20° to 90°. The morphology and cross-sectional images of thin films electroplated from deep eutectic solvents were observed by a scanning electron microscopy (SEM, JEOL JSM-IT100), the chemical composition of thin films were analyzed using an energy dispersive spectrometer (EDS). The crystalline structure of the thin films was analyzed using HR-TEM (JEOL JEM-2100). To understand the passivation behavior of the trivalent chromium coating electrodeposited from the deep eutectic solvents, X-ray photoelectron spectroscopy (XPS) was utilized (ULVAC-PHI, PHI 5000 Versa Probe). The X-ray photoelectron spectra of samples were calibrated using carbon 1s (284.6 eV). The surface of each coating was cleaned using Ar<sup>+</sup> ion sputtering for 300 s.

The measurement of potentiodynamic polarization were carried out with a standard three-electrode cell system (Autolab-PGSTAT30 potentiostat/galvanostat) under 3.5 wt. % NaCl solution and measured using a “General Purpose Electrochemical System” software at room temperature. Before potentiodynamic polarization test, the system must be stabilized at open circuit potential (OCP), the specimens must be cleaned using DI water. The analyzed potential range from −1.5 V to 0.5 V with a scanning rate of 0.5 mV s<sup>−1</sup>. The roughness of electroplating thin films deposited from deep eutectic solvents were measured by a 3D surface profilometer (Chroma 7503, Taiwan), each sample was measured five times and calculated an average value. The electrochemical impedance spectroscopy (EIS) of specimens were also analyzed in 3.5 wt. % NaCl solution. The EIS test were measured at the open circuit potential and ambient temperature with a voltage amplitude of 10 mV in the frequency range from 10<sup>−2</sup> Hz to 10<sup>5</sup> Hz for 24 h, the data processing was carried by ZSimpWin3.21 software.

### 3. RESULTS AND DISCUSSION

As shown in Fig. 1(a), the chromium thin film electrodeposited from trivalent chromium deep eutectic solvents without adding water form many crater-like holes (sample code: C1).

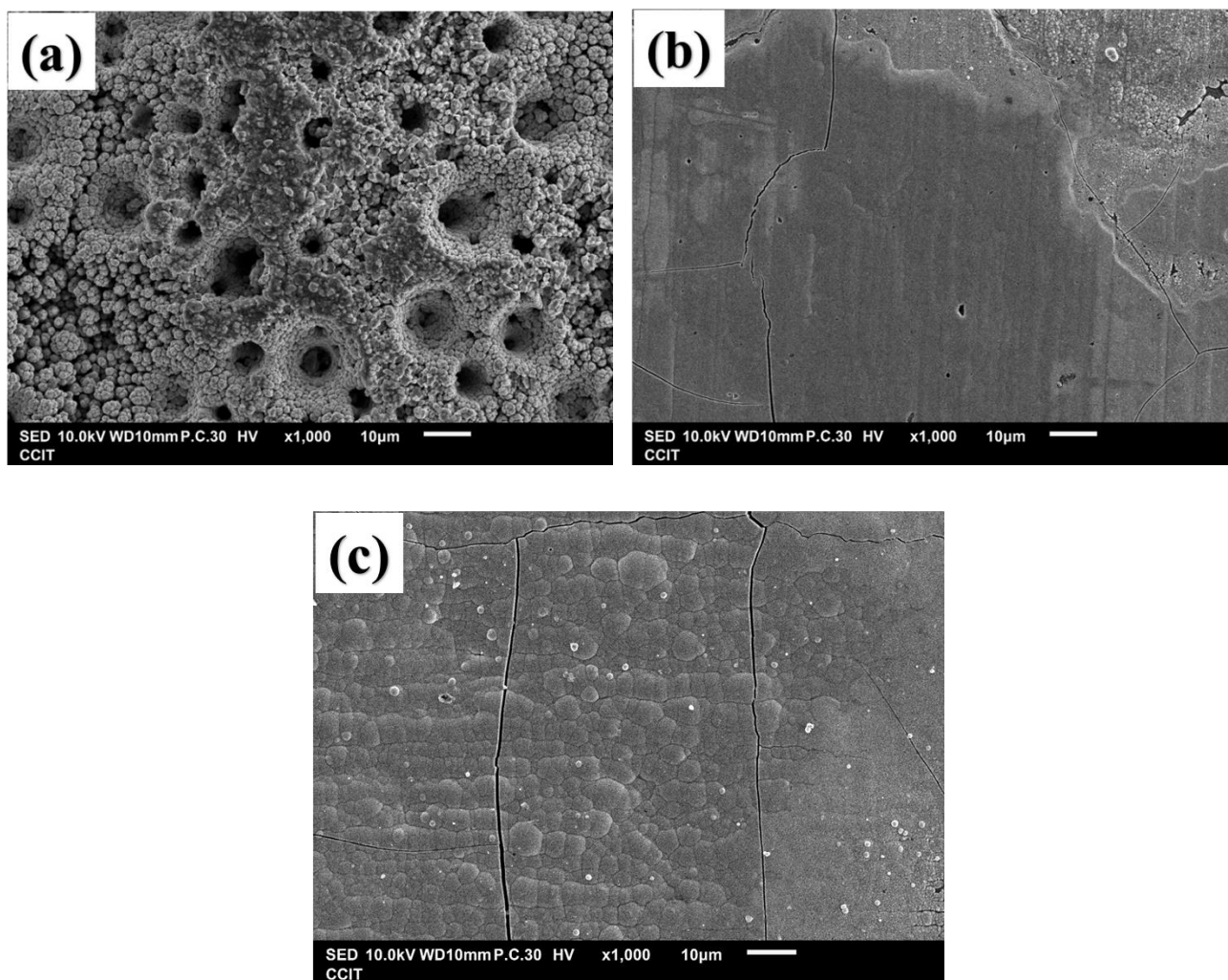
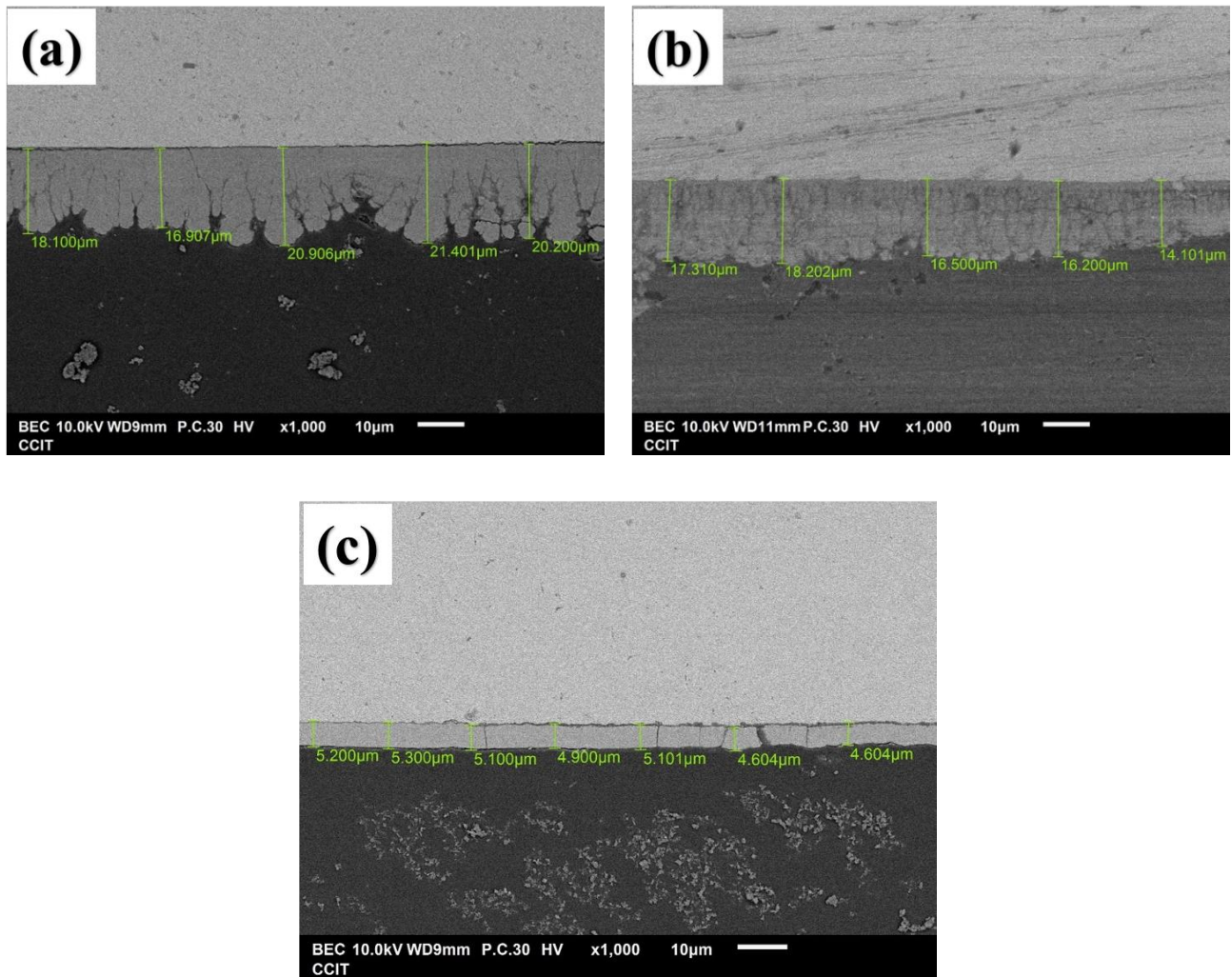


**Figure 1.** SEM morphology of Cr thin films electrodeposited from the deep eutectic solvents (a) specimen “C1”, (b) specimen “C2”, (c) specimen “C3”.

These holes are formed by the hydrogen evolution reaction in the cathode that caused by the highly viscosity of deep eutectic solvents without adding water [14]. Fig. 1(b) shows the morphology of thin films electrodeposited from the deep eutectic solvents with adding 15 wt.% water, the surface of the thin film is quite smooth, but there are still many areas where pores and loose structures are formed (sample code: C2). Fig. 1(c) shows the morphology of thin films electrodeposited from the deep eutectic solvents with adding 15 wt.% water with ammonium formate, the pores caused by hydrogen evolution reaction disappeared, and the thin film showed a complete morphology dominated by a nodules structure (sample code: C3).

Fig. 2(a) presents the cross-sectional SEM photograph of specimen “C1”, the thin film is deposited in a columnar stack and forms many gaps perpendicular to the substrate, although the average

thickness of the coating reaches 18.7  $\mu\text{m}$ , but the thin film is a loose structure and has a rough surface. Fig. 2b shows the SEM image of the cross-section of specimen “C2”, it shows that the deposition type of the film is still columnar stacking, the gap still perpendicular to the substrate but becomes finer, the average thickness of the thin film decreases to 16.4  $\mu\text{m}$  and still maintains a loose structure.



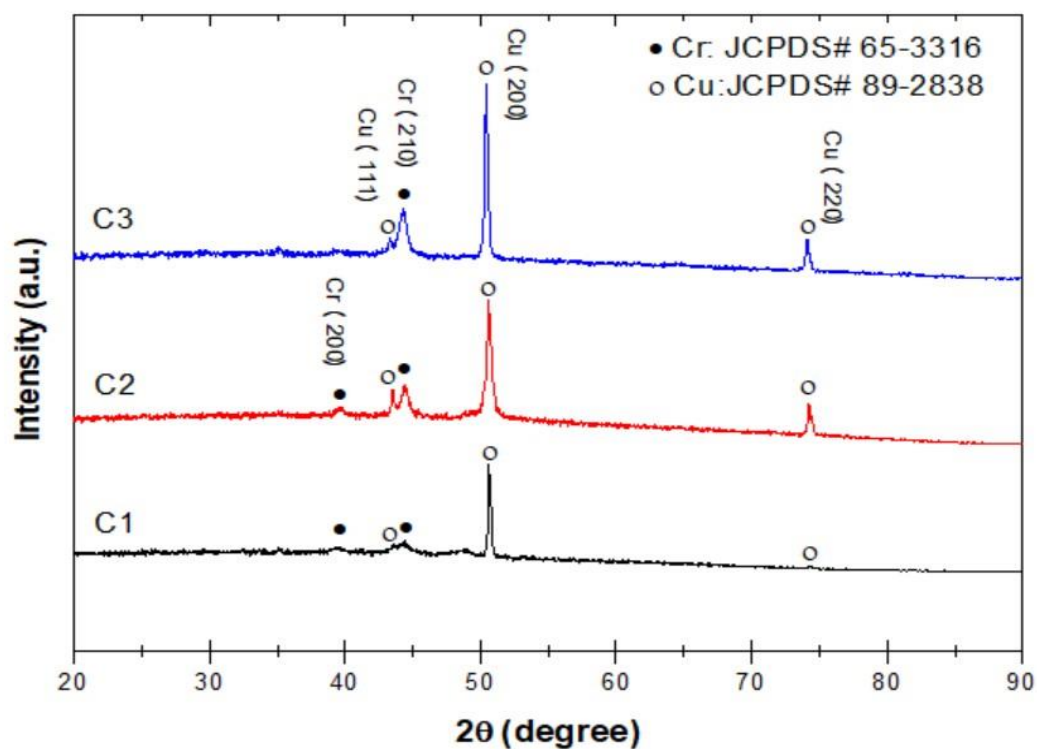
**Figure 2.** SEM cross-sectional images of Cr thin films electrodeposited from the deep eutectic solvents (a) specimen “C1”, (b) specimen “C2”, (c) specimen “C3”.

Fig. 2c is a cross-sectional SEM photograph of specimen “C3”, showing that the deposition mode of the film changed to a typical electrodeposited dense-packed, the gaps of film perpendicular to substrate is disappeared, but cracks were formed due to internal stress, and the average thickness of the film was reduced to 5.1  $\mu\text{m}$ .

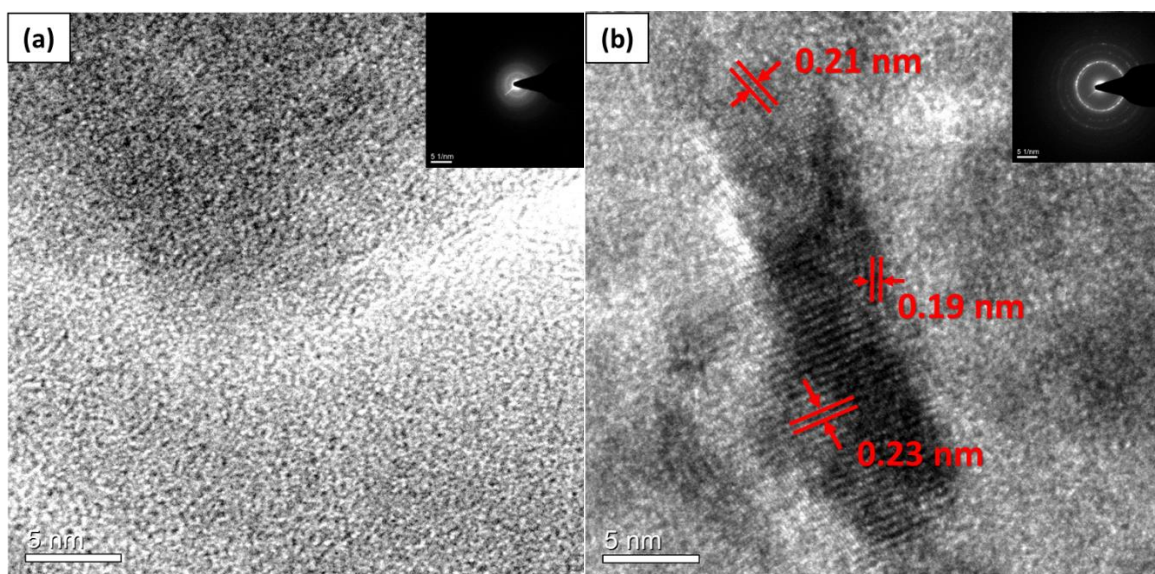
Fig. 3 shows the XRD pattern of “C1”, “C2” and “C3”, respectively. The diffraction peaks of copper substrate is still keep very clear. The diffraction intensity of (200) plane of Cr is very weak in all specimens. The greatest intensity of (210) plane of Cr occurred at the specimen “C3”, the lowest

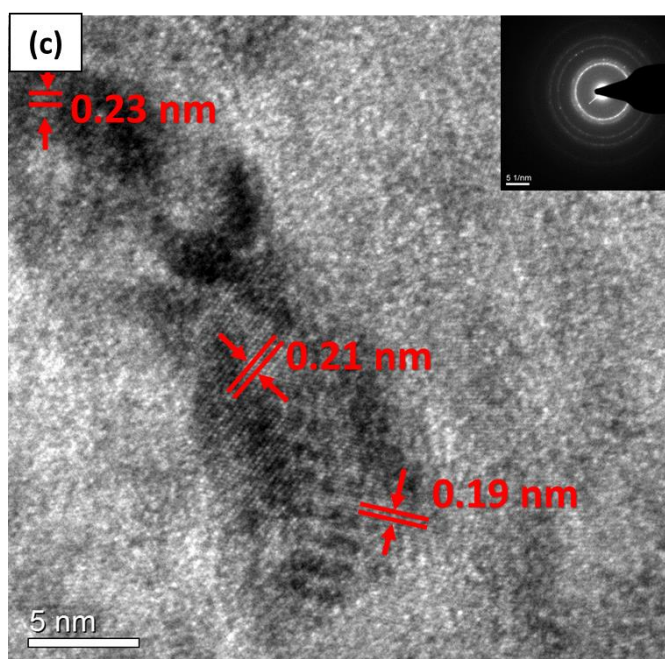


diffraction intensity occurred at the specimen “C1”. The result of XRD indicated that the “C3” has the best Cr crystalline structure.



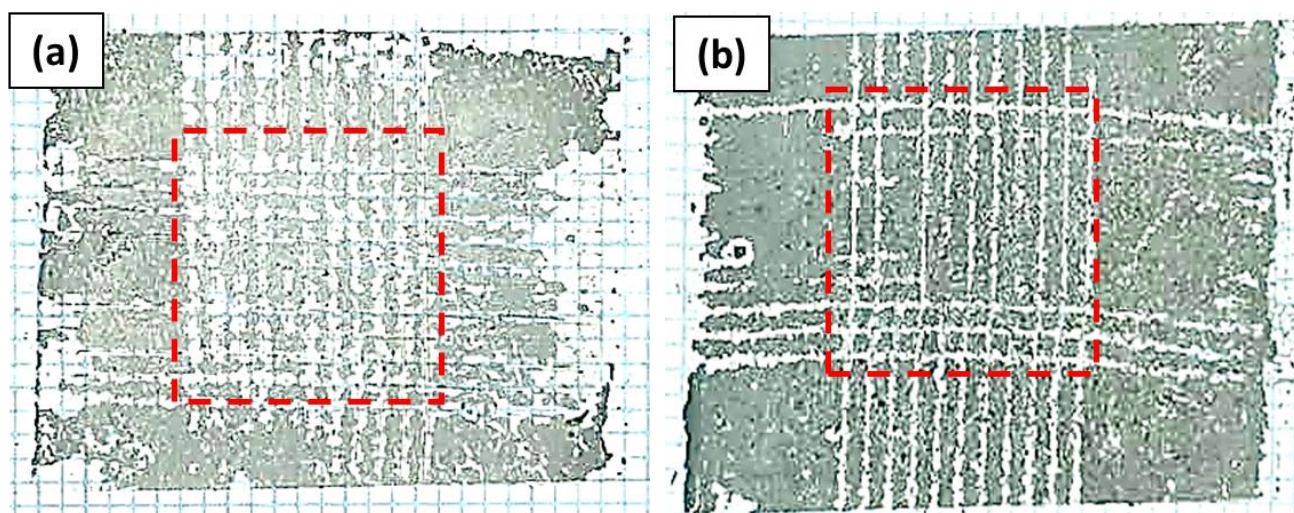
**Figure 3.** The XRD patterns of Cr thin films electrodeposited from the deep eutectic solvents (a) specimen “C1”, (b) specimen “C2”, (c) specimen “C3”.



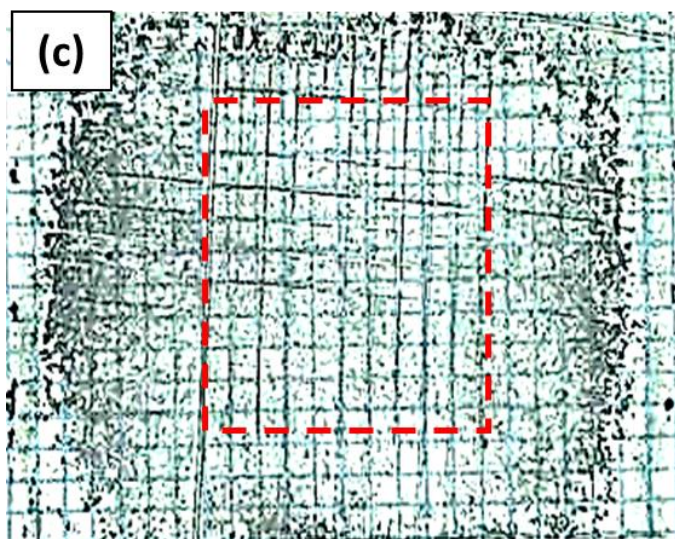


**Figure 4.** The TEM images of chromium thin films electrodeposited from the deep eutectic solvents (a) specimen "C1", (b) specimen "C2", (c) specimen "C3" (including SADE pattern).

Fig. 4 presents HR-TEM images and SADE patterns of "C1", "C2" and "C3", respectively. The corresponding electron diffraction pattern characterized by a diffuse halo showing its amorphous characteristics of "C1". Both of the SADE pattern of "C2" and "C3" has the characteristics of nano-crystalline structure belong to the Miller's index (200), (210) and (211) of chromium, respectively. The measured d-space is 0.19, 0.21 and 0.23 nm which is corresponding to the d-space of (200), (210) and (211) plane of chromium.



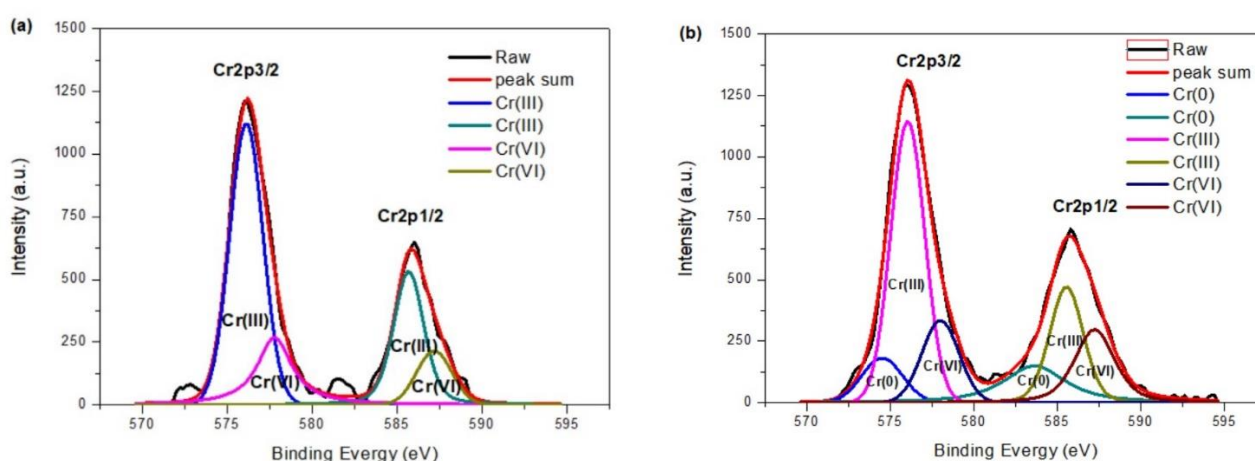




**Figure 5.** The adhesion test of chromium thin film electrodeposited from deep eutectic solvents bath: (a) specimen “C1”, (b) specimen “C2”, (c) specimen “C3”.

The adhesion of thin film of “C1”, “C2” and “C3” was evaluated using the cross-hatch method, the test result are shown in Fig. 5. According to the ASTM D-3359 classification, both the thin film of “C1” and “C2” has a very bad adhesion strength which was classified as Class (0B), thin film of “C3” has the best adhesion strength which was classified as Class (4B). The bad adhesion strength of “C1” and “C2” can be attributed to the loose structure of thin films (see Fig. 2(a),(b)).

Fig. 6 shows the XPS spectrum corresponding to the chromium core level spectra of the Cr thin films electrodeposited from deep eutectic solvents without adding water (C1), added 15 wt.% water (C2), added 15 wt.% water and ammonium formate (C3), respectively.





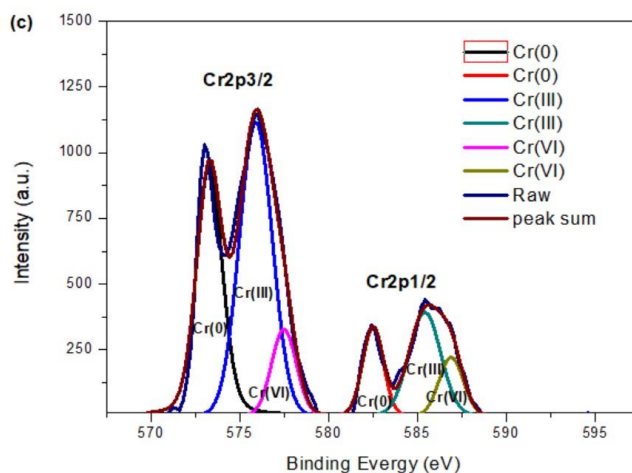


**Figure 6.** The de-convolution curve fitting analyses on the binding energy peaks of Cr elements in the measured XPS spectra of the Cr thin films electrodeposited from the deep eutectic solvents: (a) specimen “C1”, (b) specimen “C2”, (c) specimen “C3”.

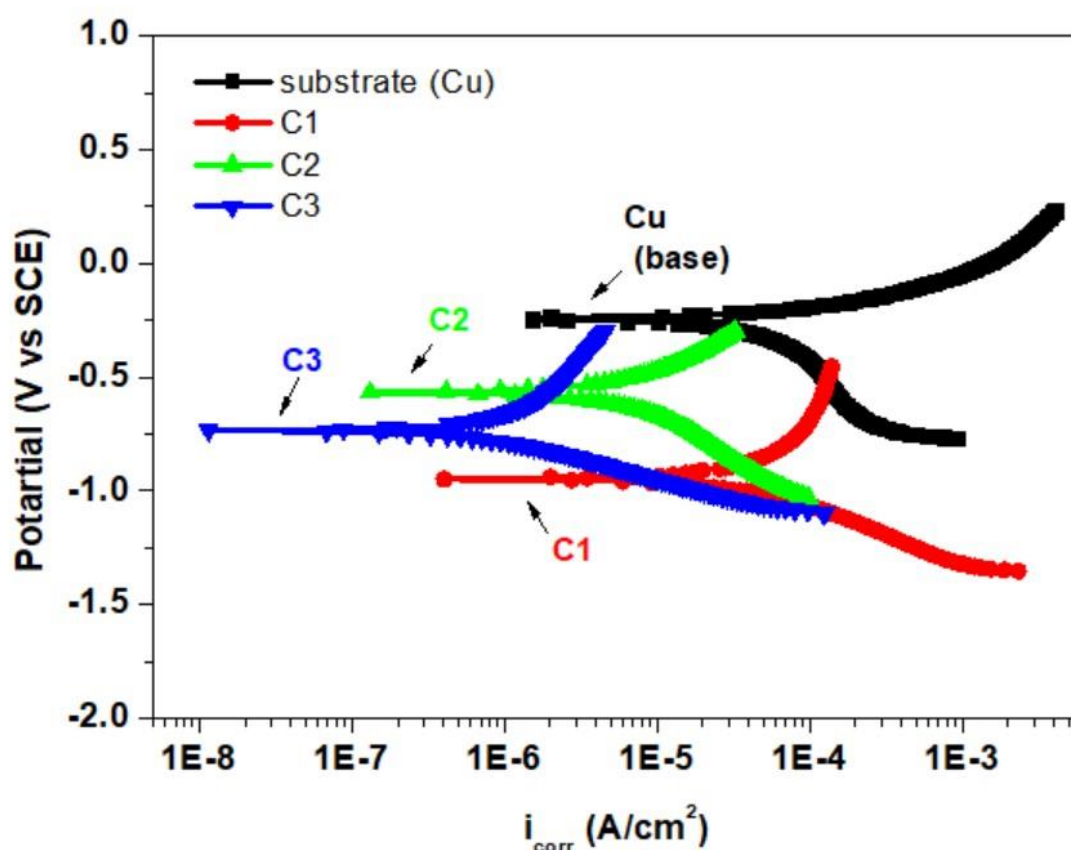


**Figure 7.** Potentiodynamic polarization curves of copper substrate, specimen C1, specimen C3 and specimen C3 in 3.5 wt.% NaCl solution.

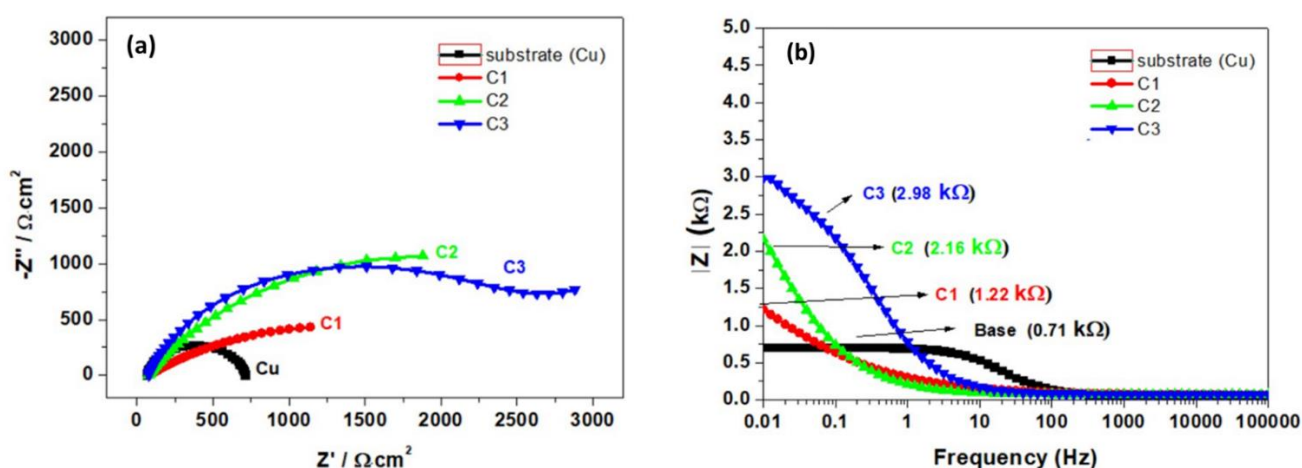
The binding energy of  $\text{Cr}2p_{3/2}$  and  $\text{Cr}2p_{1/2}$  orbitals in the “C1” specimen, “C2” specimen and “C3” specimen is composed of  $\text{Cr}_0=583.5$  eV [18],  $574.4$  eV [18],  $\text{Cr}^{3+}=586.1$  eV [19],  $576.2$  eV [20,21] and  $\text{Cr}^{6+}=587.6$  eV [22],  $578.4$  eV [23]. The intensity of XPS spectra of  $\text{Cr}^{3+}$  and  $\text{Cr}^{6+}$  are similar

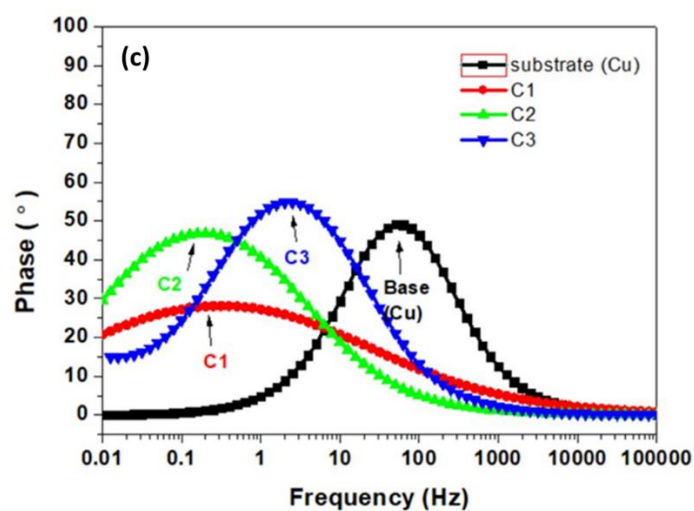
regardless of whether there is water in the deep eutectic solvents, this indicated that the surface of chromium thin film form oxide layer including  $\text{CrO}_3$  layer and  $\text{Cr}_2\text{O}_3$  layer after or in electroplating process. The intensity of  $\text{Cr}_0$  of the specimen “C1” is significantly small, the intensity of  $\text{Cr(III)}$  is significantly higher than that of  $\text{Cr(VI)}$ , indicating the composition of “C1” is composed with  $\text{CrO}_3$  and  $\text{Cr}_2\text{O}_3$  compounds (Fig. 6(a)). When the 15 wt.% water added into deep eutectic solvents (“C2”), the intensity of  $\text{Cr}_0$  formed in the Cr thin film become greater, this phenomenon can be attributed to the addition of water will improve the conductivity of the deep eutectic solvents and promote the reduction of chromium ions to metallic chromium ( $\text{Cr}_0$ ) at the cathode [14]. When the deep eutectic solvents added water and ammonium formate, the electrodeposited Cr thin film the intensity of  $\text{Cr}_0$  is almost the same with the intensity of  $\text{Cr(III)}$ , indicating the addition of ammonium formate will promote the reduction reaction of Cr ions.

Fig. 7 shows the polarization curves of copper substrate, “C1”, “C2” and “C3”, the value of  $E_{\text{corr}}$  and  $i_{\text{corr}}$  are also shown in Table 2.

**Table 2.** Results of potentiodynamic polarization tests of copper substrate, specimen C1, specimen C3 and specimen C3 in 3.5 wt.% NaCl solution.

	$I_{\text{corr}} (\text{A/cm}^2)$	$E_{\text{corr}} (\text{V})$
Copper substrate	$2.53 \times 10^{-5}$	-0.243
C1	$3.05 \times 10^{-5}$	-0.952
C2	$4.02 \times 10^{-6}$	-0.575
C3	$3.69 \times 10^{-7}$	-0.734





**Figure 8.** EIS measurements of specimens “C1”, “C2” and “C3” analyzed in 3.5 wt% NaCl solution: (a) Nyquist diagram, (b) Bode plot, (c) phase angle plot.

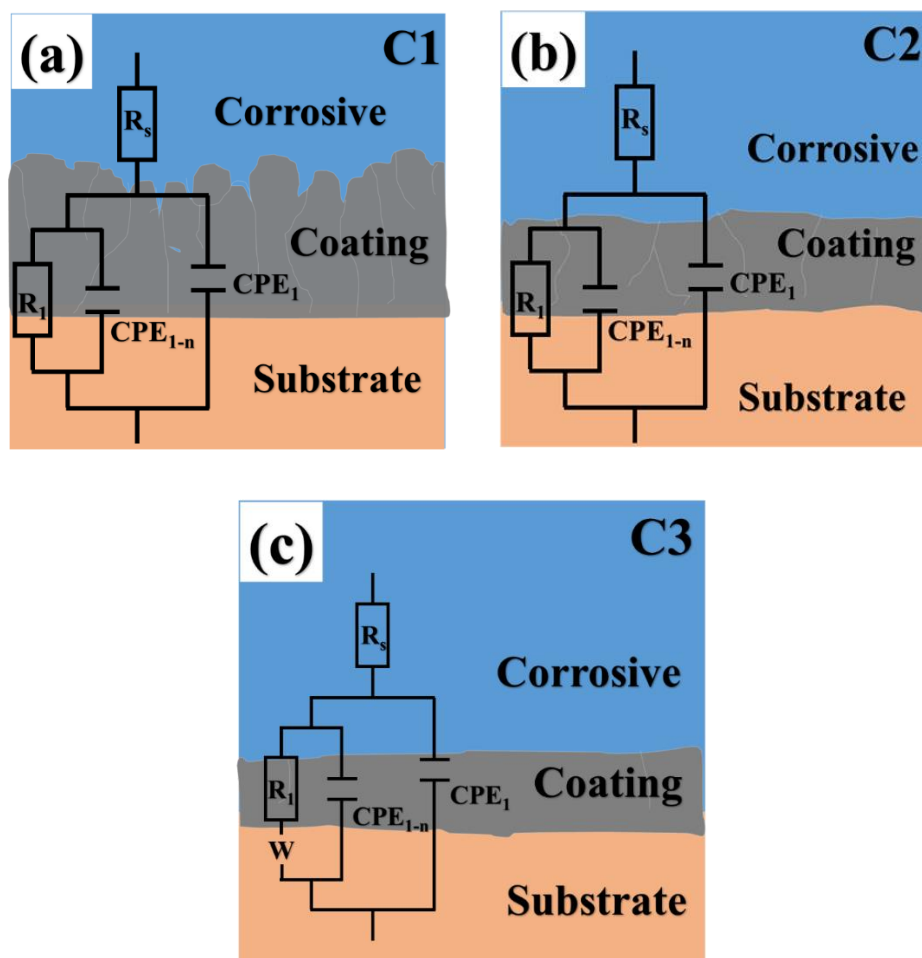


**Figure 9.** Equivalent circuits of Cr thin films electrodeposited from the deep eutectic solvents: (a) specimen “C1”, (b) specimen “C2”, (c) specimen “C3”.

The  $E_{\text{corr}}$  potential of “C1” is -0.95 V which belong the corrosion potential of Cr(VI) [14,24], the  $E_{\text{corr}}$  potential of “C2” and “C3” is between -0.5 V to -0.75 V which belong the corrosion potential of Cr(III) [25]. The  $i_{\text{corr}}$  of “C1”, “C2” and “C3” is approximately at  $3.05 \times 10^{-5}$ ,  $4.02 \times 10^{-6}$  and  $3.69 \times 10^{-7}$  A/cm<sup>2</sup>, respectively (see Table 2). Specimen “C1” has the highest  $i_{\text{corr}}$  value, indicating the thin film has the worst corrosion resistance due to its loose structure. Specimen “C3” has the lowest  $i_{\text{corr}}$  value, indicating the thin film has the best corrosion resistance due to its dense structure.

The impedance spectra of Cu substrate, specimen C1, specimen C2 and specimen C3 in 3.5 wt.% NaCl solution are showed in Fig. 8. Fig. 8(a) shows the Nyquist diagram of different specimens, “C3” has the biggest size of semicircles radii, indicating “C3” has the best corrosion resistance. Fig. 8(b) shows the Bode plot of various specimens. The impedance value  $|Z|$  at high frequency (100 Hz to  $10^5$  Hz) shows low constant values which corresponds to the response of the electrolyte resistance or surface defect [26-28], impedance values  $|Z|$  at the medium frequency region and low frequency region indicates the evolution in coating and the process at the interface of the metal/thin film [29], respectively. In frequency at  $10^{-2}$  Hz, the value  $|Z|$  of Cu substrate, specimen C1, specimen C2 and specimen C3 is 0.71 k $\Omega$ , 1.22 k $\Omega$ , 2.16 k $\Omega$  and 2.98 k $\Omega$ , respectively, indicating the “C3” specimen has the best anti-corrosion behavior at the interface of the copper/”C3” thin film. In the medium frequency region ( $10^{-2}$  Hz to 10 Hz), the value  $|Z|$  of “C3” is still greater than that of “C1” and “C2”. The lower value  $|Z|$  in the medium frequency region can be attributed to the unstable in characteristics of thin film such as the uneven thickness, cracks and loose structure [30,31]. The results of Bode plot is agreement with the observation of SEM cross-sectional images in Fig. 2., the “C1” and “C2” has loose structure. Fig. 8(c) presents the phase angle plot of various specimens, the phase angle of “C1” and “C2” occurred at lower frequency region, and the “C3” occurred at higher frequency region. At frequencies between 1 Hz and  $10^{-2}$  Hz the total impedance and phase shift can be attributed to electrochemical processes near the metal surface (e.g. oxide layers) [32-34]. Therefore, the formation of oxide layer of “C1” and “C2” should easy than that of “C3”.

Considering the microstructure characteristics and EIS analysis of the specimens “C1”, “C2” and “C3”, the models chosen for the fitting of the different specimens are depicted in Fig. 9. The equivalent circuits are commonly used on Cr thin film [35–37], where  $R_s$  is the solution resistance,  $R_1$  is the resistive responses of the interface of copper/Cr thin film or the Cr thin film, constant phase element ( $\text{CPE}_1$ ) represent the properties of Cr thin film (Fig (9a),(b)), both of “C1” and “C2” has a loose structure and the gap is vertically connected to the substrate (see Fig. 2), causing corrosion to occur at the interface. The sketches and equivalent circuits of specimen “C3” are also shown in Fig. 9(c). In addition to  $R_s$ ,  $R_1$  and  $\text{CPE}_1$ , the equivalent circuit composition also includes  $W$  (a Warburg impedance element). It can be seen that the thin film of “C3” has a dense and one-layer structure. The equivalent circuit data of specimen “C1”, “C2” and “C3” measured in 3.5 wt.% NaCl solution are shown in Table 3.



**Table 3.** Equivalent circuit data of specimen “C1”, “C2” and “C3” in 3.5 wt.% NaCl solution

R(QR) type	$R_s$ ( $k\Omega \cdot cm^2$ )	$CPE_1$ ( $mF \cdot cm^{-2}$ )	$CPE_{1-n}$ ( $F \cdot cm^{-2}$ )	$R_1$ ( $k\Omega \cdot cm^2$ )	
copper substrate	0.06	2.9	0.84	0.65	
C1	0.08	173.4	0.62	2.48	
C2	0.07	175.2	0.73	3.72	
R(Q(RW)) type	$R_s$ ( $k\Omega$ )	$CPE_1$ ( $mF \cdot cm^{-2}$ )	$CPE_{1-n}$ ( $F \cdot cm^{-2}$ )	$R_1$ ( $k\Omega \cdot cm^2$ )	W ( $kF \cdot cm^{-2}$ )
C3	0.08	26.7	0.81	2.47	4.64

#### 4. CONCLUSIONS

In this study, the effect of ammonium formate addition on the microstructure and the corrosion resistance of Cr thin film deposited on copper have been investigated. The microstructure of the Cr thin films electrodeposited from deep eutectic solvents without added water (C1) and added 15 wt.% water (C2) has a loose structure and the gaps of film is perpendicular to substrate, leading to the corrosion factors directly attack the substrate, their  $i_{corr}$  value is approximately at  $3.05 \times 10^{-5}$  and  $4.02 \times 10^{-6}$  A/cm<sup>2</sup>, respectively. The Cr thin film electrodeposited from the deep eutectic solvents added 15 wt.% water with ammonium formate (specimen C3) has the lowest  $i_{corr}$  approximately at  $3.69 \times 10^{-7}$  A/cm<sup>2</sup>, the best corrosion resistance of “C3” can be attributed to a dense structure of thin film. Electrochemical impedance spectroscopy (EIS) has been applied to evaluate the influence of the addition of ammonium formate in deep eutectic solvents on the electrochemical response of the Cr thin film in 3.5 wt.% NaCl solution. The EIS result indicating that the corrosion behavior of “C1” and “C2” occurred at the interface of copper/Cr thin film due to the loose structure of Cr thin film, the “C3” occurred at the dense Cr thin film which can protect copper substrate from a corrosion.

#### References

1. E.L. Smith, A.P. Abbott, K.S. Ryder, *Chem. Rev.*, 114 (2014) 11060–11082.
2. Z.W. Wang, J.J. Ru, Y.X. Hua, D. Wang, J.J. Bu, *J. Electrochem. Soc.*, 167 (2020) 082504.
3. A.Y.M. Al-Murshedi, J.M. Hartley, A.P. Abbott, K.S. Ryder, *Trans. Inst. Metal Finish.*, 97 (2019) 321.
4. D.V. Wagle, H. Zhao, G.A. Baker, *Accounts Chem. Res.*, 47 (2014) 2299.
5. F. I. Danilov, V. S. Protsenko, V. O. Gordienko, S. C. Kwon, J. Y. Lee, M. Kim, *Appl. Surf. Sci.*, 257 (2011) 8048.
6. H.H. Sheu, M.H. Lin, S.Y. Jian, T.Y. Hong, K.H. Hou, M.D. Ger, *Surf. Coat. Technol.*, 350 (2018) 1036.
7. A. Liang, Q. Liu, B. Zhang, L. Ni, J. Zhang, *Mater. Lett.*, 119 (2014) 131.
8. K.S. Nam, K.H. Lee, S.C. Kwon, D. Y. Lee, Y.S. Song, *Mater. Lett.*, 58 (2004) 3540.
9. L.S. Bobrova, F.I. Danilov, V.S. Protsenko, *J. Mol. Liq.*, 223 (2016) 48.
10. Elisabete S.C. Ferreira, C.M. Pereira, A.F. Silva, *J. Electroanal. Chem.*, 707 (2013) 52.
11. S. Eugénio, C.M. Rangel, R. Vilar, A.M. Botelho do Rego, *Thin Solid Films*, 519 (2011) 1845.

12. H. Khani, J.F. Brennecke, *Electrochem. Commun.*, 107 (2019) 106537.
13. V.S. Protsenko, L.S. Bobrova, A.A. Kityk, F.I. Danilov, *J. Electroanal. Chem.*, 864 (2020) 114086.
14. T.T. Lin, H.H. Sheu, M.D. Ger, *Int. J. Electrochem. Sci.*, 16 (2021) 211055.
15. H.H. Sheu, C.H. Lin, S.Y. Jian, H.B. Lee, B.R. Yang, M.D. Ger, *Int. J. Electrochem. Sci.*, 11 (2016) 7099.
16. H.H. Sheu, Y.R. Chen, M.D. Ger, *Int. J. Electrochem. Sci.*, 15 (2020) 2851.
17. N. Wagner, *J. Appl. Electrochem.*, 32 (2002) 859.
18. T.J. Lin, H.H. Sheu, C.Y. Lee, H.B. Lee, *J. Alloys Compd.*, 867 (2021) 159132.
19. C.Y. Lee, T.J. Lin, H.H. Sheu, H.B. Lee, *J. Mater. Res. Technol.*, 15 (2021) 4880.
20. R. Merryfield, M.P. McDaniel, G. Parks, *J. Catal.*, 77 (1982) 348.
21. A.B. Gaspar, C.A.C. Perez, L.C. Dieguez, *Appl. Surf. Sci.*, 252 (2005) 939.
22. Z. Ren, X. Xu, X. Wang, B. Gao, Q. Yue, W. Song, L. Zhang, H. Wang, *J. Colloid Interface Sci.*, 468 (2016) 313.
23. N. Benito, D. Díaz, L. Vergara, R. Escobar Galindo, O. Sánchez, C. Palacio, *Surf. Coat. Technol.*, 206 (2011) 1484.
24. Z.H. Liu, C. Liu, Z.F. Xu, J. Rong, X.H. Yu, Y. Zhang, *Int. J. Electrochem. Sci.*, 13 (2018) 6473 - 6483.
25. H.H. Sheu, Y.R. Chen<sup>1</sup>, M.D. Ger, *Int. J. Electrochem. Sci.*, 15 (2020) 2851.
26. M. E. Orazem and B. Tribollet, *Electrochemical Impedance Spectroscopy*, Hoboken, NJ, USA: John Wiley & Sons Inc., 2008.
27. M.L. Zheludkevich, R. Serra, M.F. Montemor, K.A. Yasakau, I.M.M. Salvado, M.G.S. Ferreira, , *Electrochim. Acta*, 51 (2005) 208.
28. Paul J. Denissen, S. J. Garcia, *Electrochimica Acta*, 293 (2019) 514.
29. N.D. Nam, M.J. Kim, D.S. Jo, J.G. Kim, D.H. Yoon, *Thin Solid Films*, 545 (2013) 380.
30. Y. Chen, N.G. Rudawski, E.S. Lambers, M.E. Orazem, *J. Electrochem. Soc.*, 164 (2017) C563.
31. B. Hirschorn, M.E. Orazem, B. Tribollet, V. Vivier, I. Frateur, M. Musiani, *J. Electrochem. Soc.*, 157 (2010) C458.
32. S.J. Xia, R. Yue, R.G. Rateick Jr., V.I. Birss, *J. Electrochem. Soc.*, 151 (2004) B179.
33. H. Yasuda, Q.S. Yu, M. Chen, *Prog. Org. Coating*, 41 (2001) 273.
34. L. Wen, Y. Wang, Y. Zhou, L. Guo, J.H. Ouyang, *Corrosion Sci.*, 53 (2011) 473.
35. N.T. Wen, C.S. Lin, C.Y. Bai, M.D. Ger, *Surf. Coat. Technol.*, 203 (2008) 317.
36. C.R. Tomachuk, A.R.D. Sarli, C.I. Elsner, *Materials Sciences and Applications*, 1 (2010) 202
37. X. He, C. Li, Y. Jiang, Q. Zhu, W. Wang, C. Zhang, L. Wu, *J. Electrochem. Soc.*, 162 (2015) D435